AIAA SciTech Forum
23-27 January 2023, National Harbor, MD & Online
AIAA SCITECH 2023 Forum

10.2514/6.2023-1410

Novel Methods to Detect Trace Quantities of 1-ethyl-3-methylimidazolium tetrafluoroborate

Stefan Bell*, Carl Geiger†, Ben Inbar‡, Mark Pfeifer§, and Elaine Petro¶
Cornell University, Ithaca, New York, 14850

Reliable surface detection of deposited propellant is critical to studying overspray, a primary lifetime limiting mechanism of electrospray thrusters. This work explores four methods for the detection of 1-ethyl-3-methylimidazolium tetrafluoroborate (EMI-BF_4), a room-temperature ionic liquid commonly used as propellant in electrospray thrusters: fluorescent spectroscopy, energy-dispersive X-ray spectroscopy, nonvolatile residue spectroscopy, and Fourier transform infrared spectroscopy. Successful detection of EMI-BF_4 deposited onto a gold plated quartz crystal substrate by an electrospray source is demonstrated using energy-dispersive X-ray spectroscopy. Nonvolatile residue spectroscopy is shown to be capable of detecting highly diluted EMI-BF_4. Fourier transform infrared spectroscopy was performed on a large drop of EMI-BF_4 and differentiation between similar molecules was established. Initial surface contamination studies using UV-Vis fluorescent spectroscopy to detect the presence of EMI-BF_4 on quartz crystal substrates are also conducted.

I. Introduction

Electrospray thrusters are a class of electric propulsion that is particularly well suited for small satellites, attitude control, and high Δv missions. Electrospray thrusters provide high precision, throttleable, micronewton level thrust at high specific impulse. These systems are highly scalable, compact, and operate at low power, uniquely positioning electrosprays as an enabling technology for micro and nanosatellites, which would have otherwise not have onboard propulsion.

Electrosprays are theoretically capable of operating for tens of thousands of hours, though this has not been demonstrated, and lifetime modeling highlights several failure modes [1]. Overspray of particles in the ion plume due to beam divergence collide with the anode, causing a thin film to build up. This thin film will grow until enough material is present to electrically bridge the anode and cathode, causing a short circuit. This catastrophic failure mode has been identified as a primary lifetime limiting factor for electrospray thrusters [2][1]. Plume simulations have demonstrated this overspray, especially in neutral populations, though experimental validation is still required[3]. Direct measurements of deposited propellant will be necessary to develop accurate thruster lifetime predictions.

Traditional methods for characterizing electrospray plumes typically make use of electrostatic analyzers, leveraging the high charge to mass ratio of ions in the plume [4]. Retarding potential analyzers (RPA) use a series of high transparency electrodes to systematically filter ions by energy. The ions that pass through the electrodes are read by a current collector, producing an energy profile of the ion plume. Time of flight mass spectroscopy (TOF-MS) measures the current collected at the end of a flight tube from a pulsed electrospray source, producing a mass profile of the charged species present in the plume. Since the plume will contain many fragments and neutral particles that may carry no charge, traditional diagnostics are not suitable and alternative methods are required. This work aims to test the viability of several surface contamination detection diagnostics, including fluorescence spectroscopy, energy-dispersive X-ray spectroscopy, and nonvolatile residue spectroscopy, for analyzing deposited propellant from an electrospray ion source.

*PhD Student, Mechanical and Aerospace Engineering, 458 Upson Hall
†PhD Student, Mechanical and Aerospace Engineering, 568 Upson Hall, AIAA Member
‡Research Assistant, Mechanical and Aerospace Engineering, 458 Upson Hall
§CCMR Bard Hall Shared Facility Manager, 113 Thurston Hall
¶Assistant Professor, Mechanical and Aerospace Engineering, 461 Upson Hall, AIAA Member

II. Methods

A. Fluorescence Spectroscopy

Fluorescence spectroscopy uses photon absorption to excite the valence electrons of a molecule to jump discrete energy levels [5]. When the electron returns from a high energy state, a photon is emitted. This process is demonstrated in Fig. 1. For small molecules, fluorescence can be predicted easily, but with large molecules with bonds, fluorescence is usually impossible to describe analytically. By changing the excitation laser wavelength and observing the photo-emission, an emission-excitation map can be generated. This technique does not necessarily determine anything about the structure of molecule, just the relationship between photon absorption and emission.

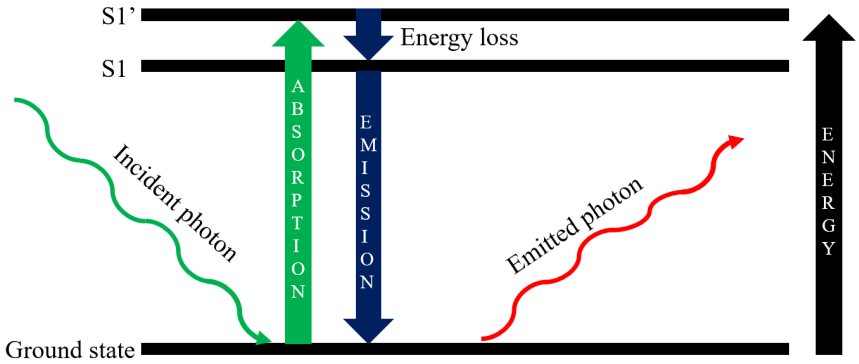

Fig. 1 Jablonski diagram of the phenomenon of fluorescence.

Fluorescence spectroscopy is commonly used in analysis of dissolved solutions of biological molecules and thin films. The Cornell Center for Materials Research (CCMR) shared facilities includes the Edinburgh FLS 1000 Fluorescence Spectrophotometer. The instrument reports a calibrated number of counts from the photo-detector and has no information about total energy input or output from the fluorescence, so it can only detect the presence of the fluorescing material. Therefore, because fluorescence spectroscopy is fast when the excitation peak is known, this technique is best suited for identifying areas of contamination for further analysis if desired. For this study, transparent substrates like glass and quartz were tested, but ultimately rejected as a substrate for deposition due to unfavorable diffraction properties interfering with the fluorescent signal. The experiments began with a broad range of excitation wavelengths, between 200 nm and 600 nm. This range was quickly narrowed down to the current region of interest between 260 nm and 380 nm. Since the range of interest is rather narrow, a simpler implementation of the fluorescence spectrophotometer for the exclusive detection of EMI-BF_4 is feasible. Results for fluoresence mapping and sample analysis are provided in Section III.

B. Energy-dispersive X-ray spectroscopy

Energy-dispersive X-ray spectroscopy (EDX) works by bombarding a sample with an electron beam and measuring the X-rays produced, as seen in Fig. 2. These X-rays will generate a spectra which identifies the presence of some elements. These spectra gives no information on the structure of the molecule, nor is it good at detecting low atomic mass elements like boron and hydrogen. Through the use of CCMR's Scanning Electron Microscope (SEM), EMI-BF_4 has been detected by looking for the presence of fluorine. This element does not readily occur in common materials (unlike carbon for example), so the detection of fluorine indicates that some EMI-BF_4 is present. EDX analysis is traditionally used to verify the presence of elements in a material, such as dopants in a semiconductor, especially since the electrons can tunnel into a substrate to reveal subsurface information. In the case of EMI-BF_4, this tunneling is not desired, and likely affects the minimum detection concentration.

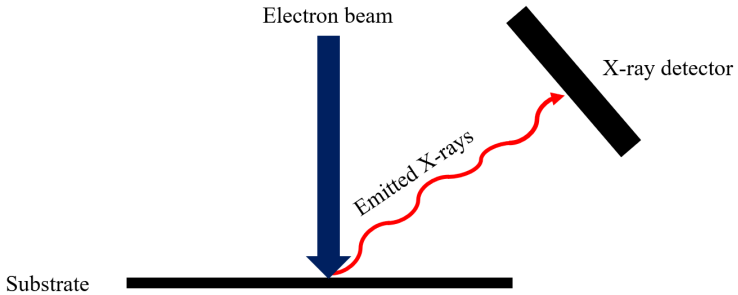

Fig. 2 Diagram of an EDX system.

C. Nonvolatile Residue Spectrometry

Nonvolatile Residue (NVR) Spectroscopy is a method of measuring the mass and composition of a surface contaminant. Traditionally, NVR includes a measurement of the mass of the residue when the mass of the residue exceeds the detection threshold of the accompanying microbalance (typically 1 µg). The residue can then be loaded into an electrospray mass spectrometer where it is ionized and accelerated down a time-of-flight tube until it reaches a detector. The time a particular ion takes to travel the length of the tube is dependent on its charge to mass ration and the accelerating voltage, determining its molecular composition. The Biotechnology Resource Center of Cornell Institute of Biotechnology (BRC) performed electrospray mass spectrometry (ESI-MS) using a Sciex X500B TOF-MS. In order to establish a baseline for the detection of EMI-BF_4, a dilution of a pure sample was fed into the TOF-MS and a full spectra was acquired in both the positive and negative ion modes.

D. Fourier Transform Infrared Spectroscopy

Fourier Transform Infrared (FTIR) Spectroscopy is a spectral analysis technique used to identify a variety of material properties and chemical bonds. This technique is traditionally used to non-destructively measure damage on aircraft surface structures [6], or crystal orientation in recycled plastics [7]. FTIR measures the reflectance or absorbance of a material over a broad wave number range. The resulting spectrum can be used to derive the presence of chemical bonds, molecular orientation, or the presence of defects. Using CCMR's Bruker Vertex V80V Vacuum FTIR system, Attenuated Total Reflectance (ATR) was measured for a liquid sample of EMI-BF_4. The spectrum was compared to a library of many chemicals, allowing for sample identification.

E. Sample Preparation

Recent electrospray characterization studies have shown the use of quartz crystal microbalances (QCM) to be a promising method for measuring neutral mass-flux[8]. Therefore, the quartz crystal used in QCMs was chosen as a the substrate on which propellant from an electrospray plume would be deposited. QCMs measure the resonant frequency change of a piezoelectric quartz crystal, which is directly related to the change in mass on the crystal surface, so verifying and characterizing propellant surface deposition will be an important step toward validating the use of QCMs for electrospray mass flux analysis.

A recent study measured an increase in QCM frequency (indicative of surface mass removal) when exposed to a high energy plume, and a decrease in QCM frequency (indicative of mass deposition) when exposed to a low energy plume[9]. Two gold coated quartz crystals were each exposed to plumes accelerated by differing electric potentials produced by the externally wetted, single tungsten emitter electrospray source shown in Fig. 3 under vacuum (1 µTorr) using a Keithley 2657A SMU and Stanford Research Systems PS350 High Voltage Power Supply. One was exposed to a high energy plume accelerated at nominal firing potential, -2670 V, for approximately 17 hours with an average emitted current of -535 nA. The other was exposed to a low energy plume accelerated to nominal firing potential and then decelerated, traveling across a net -30 V, for approximately 4 hours with an average emitted current of -77 nA.

TOF-MS data indicates an externally wetted tungsten emitter operating in the negative ion mode produces an ion plume consisting of roughly 50% monomers, BF_4^- (86.6 Da) and 50% dimers, (EMI-BF_4)BF_4^- (284.8 Da)[10]. Using this data, the approximate emitted mass from the high energy plume is 63.12 µg and for the low energy plume 2.14 µg,

though it is expected that the mass reaching the target will be a fraction of the emitted mass due to interception at the acceleration and deceleration electrode. A clean, unused quartz crystal is analyzed alongside the other two to serve as a base line and control. For each test, the quartz crystal was shielded while the electrospray source was not firing, ensuring EMI-BF_4 only reaches the crystal surface as an electrospray plume.

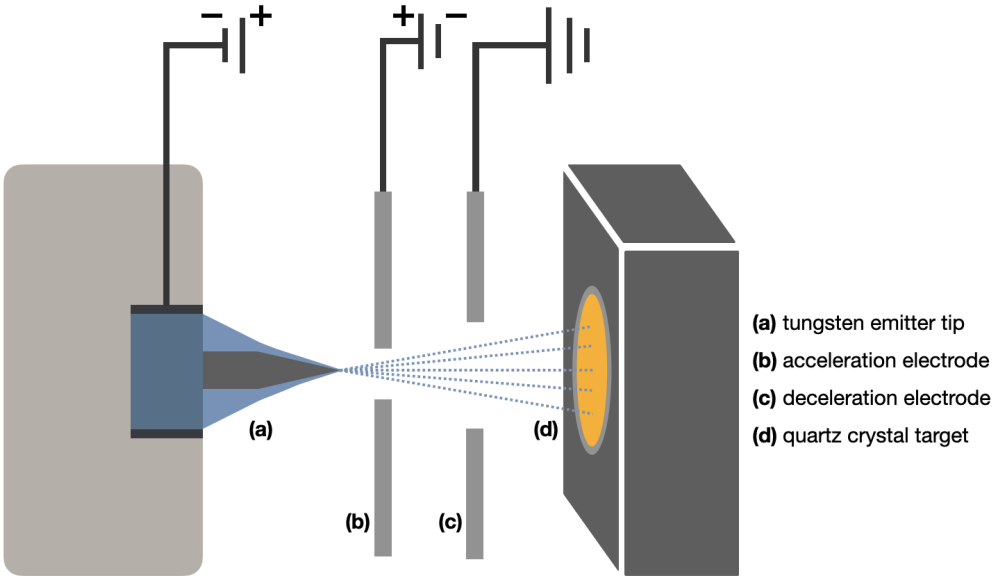

Fig. 3 Diagram of electrospray source with loaded target. Figure not to scale.

III. Results and Analysis

The samples analyzed in this study are shown in Fig. 4. The crystal exposed to a high energy ion plume developed two distinct regions, one lighter circular area, and a darker crescent area. The circular region is the subsection of the crystal that was exposed to the high energy ion plume. The crystal exposed to a low energy plume has several small droplets deposited on the surface, just barely visible to the naked eye.

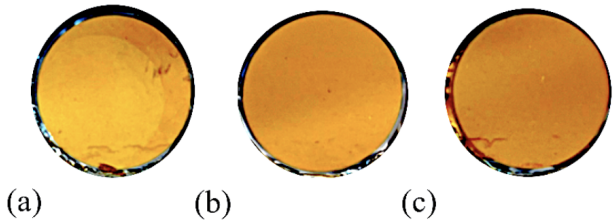

Fig. 4 (a) High energy QCM crystal, (b) Low energy QCM crystal, (c) Blank QCM crystal.

A. Fluorescence Spectroscopy

Figure 6 shows that the excitation wavelengths of interest are around 260-280 nm, with the emission occurring predominantly in the 310-360 nm region. Because some emission occurs in the lower-visible spectrum, this fluorescence can be verified visually, seen in Fig. 5. After establishing that EMI-BF_4 fluoresces, measuring the fluorescent signal from EMI-BF_4 deposited onto quartz crystals was the next step. Figure 6 also shows the emission spectra for the gold surface. This structure appears to be a Raman signal, but this must be confirmed with Eq. (1). Here, $\lambda_{excitation}$ is the excitation wavelength with units nm, λ_{Raman} is the emission wavelength in the "Raman" region with units nm, and $\Delta\nu_r$ is the Raman shift, with units nm^{-1}. Using two points along the most prominent structure at (316 nm, 286 nm) and (348

nm, 314 nm), the wavenumber shift is shown to vary by about 6%.

$$\Delta\nu_r = \frac{1}{\lambda_{excitation}} - \frac{1}{\lambda_{Raman}} \tag{1}$$

Raman signals must have a constant wavenumber shift [5]. The 6% deviation (corresponding to about 200 cm^{-1}) explains that this structure seen in Fig. 6 is not a Raman signal. While the exact phenomenon causing the near-linear structures is not known, it is likely a scattering phenomenon and may be due to some light leakage through the monochromator of the fluorescence spectrophotometer.

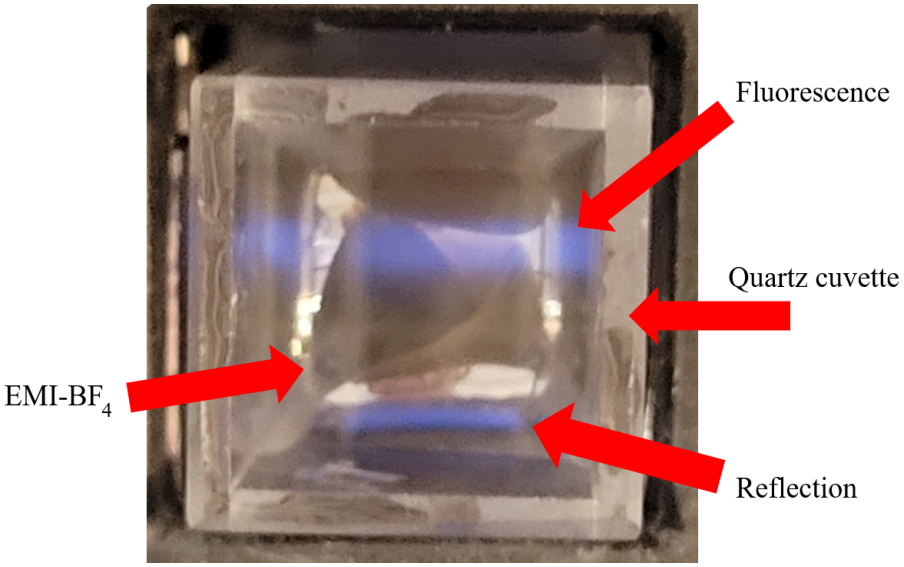

Fig. 5 Visible photo-emission of EMI-BF_4 in a quartz cuvette.

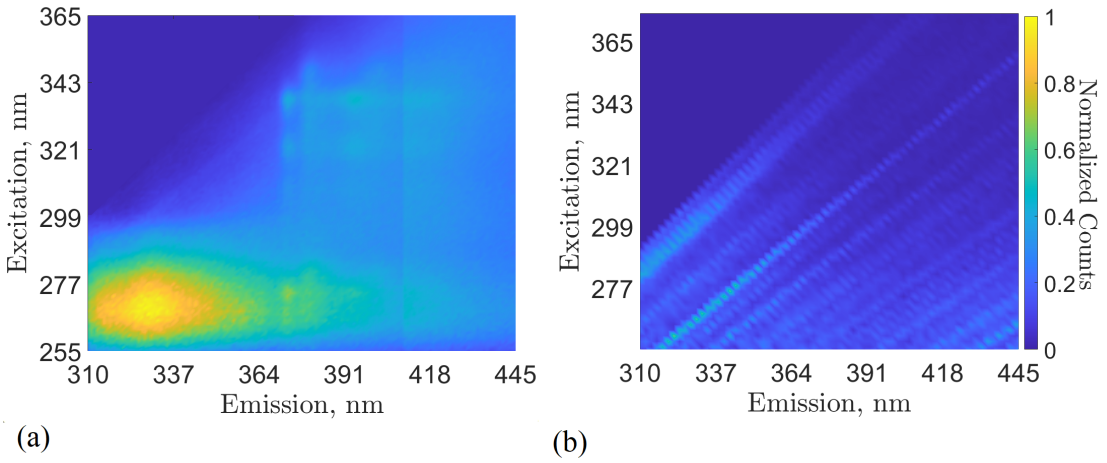

Fig. 6 (a) Emission map of EMI-BF_4 bulk fluid, (b) blank gold-plated QCM crystal.

Figure 7 shows the emission maps of the low energy QCM crystal, as well as the light and dark regions of the high energy QCM crystal seen in Fig. 4 (a) when exposed to a 2 mm^2 light beam. The gold emission structure is present in each, but the peaks are more pronounced. Figure 8 shows the emission map of the QCM crystal with deposition from low energy with the background gold subtracted. This resulting signal has a structure very similar to the original gold structure. While the exact reason is not known, the result suggests that the deposition of the EMI-BF_4 could be interacting with the gold surface in a way to inhibit its own fluorescence.

To investigate this structure, cross-correlations are used. A cross-correlation describes the similarity between two signals by sweeping one past the other and integrating the overlapped area. For a normalized cross-correlation, a sharp peak at the center with magnitude near one means that the two signals are almost identical to each other. Figure 8 shows that the original signal's cross correlation is strongly correlated to the gold signal. Figure 8 also shows that after subtracting the background signal, the resulting signal is much less correlated. The cross-correlation indicates that the resulting signal contains structures not present in the original gold background, but the background signal has not fully been removed. The presence of unique structures imply that there could be a way to measure deposition with fluorescence spectroscopy, but requires further investigation. No clear deposition has been measured through fluorescence in this work.

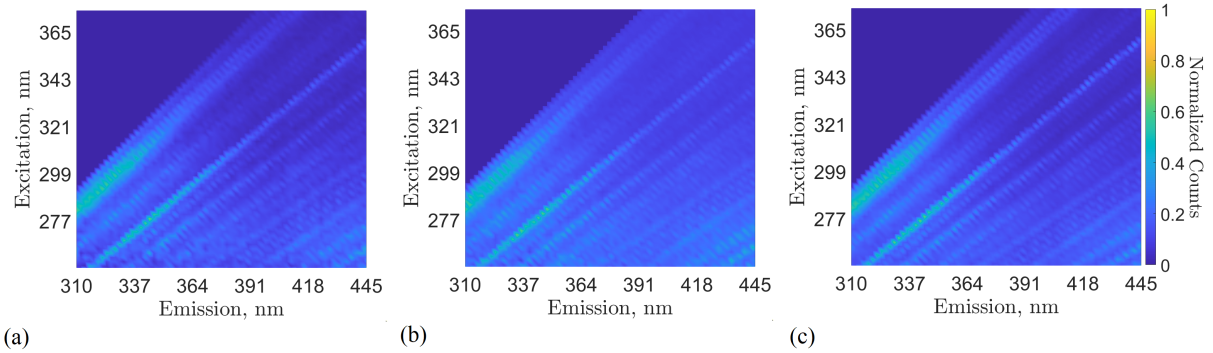

Fig. 7 (a) Emission map of a QCM crystal under low energy, (b) light region of high energy, (c) dark region of high energy.

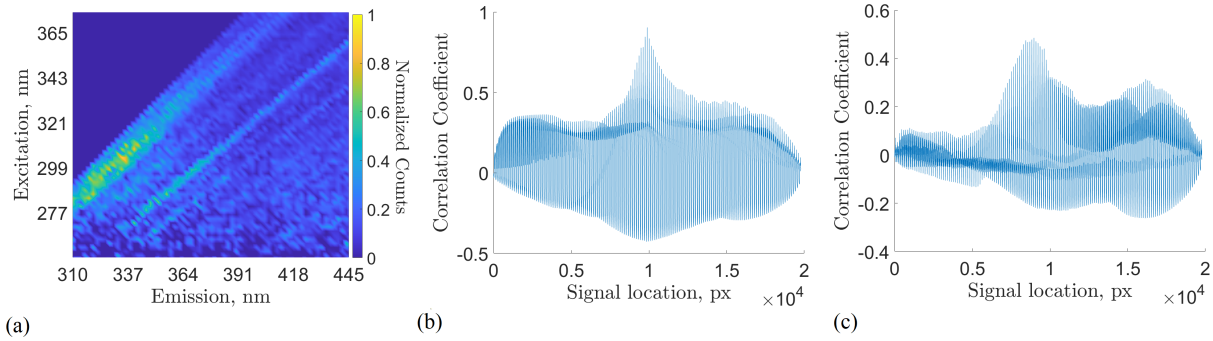

Fig. 8 (a) Emission map of low energy deposition with the gold substrate subtracted, (b) cross-correlation of the original map with the background gold, (c) cross-correlation of (a) with the gold substrate emission map.

B. EDX

All EDX measurements were collected using the Zeiss LEO 1550 FESEM. Figure 9 shows the difference between a blank QCM crystal and the QCM crystal that was exposed to high energy. The QCM crystal has its own structure with a completely conductive surface seen in Fig. 9 (b). Figure 9 (a) shows that there are areas of the surface containing small black spots, these spots can be seen towards the top with some examples highlighted. These spots have been found to be small amounts EMI-BF_4, similar to those seen in Fig. 10. There are also regions where some charge is accumulating, which could be indicative of the presence of EMI-BF_4, since gold is much more conductive than EMI-BF_4 and no other non-conductive contaminants were found.

Figure 10 shows that for low energy ion beam exposure, significant deposition occurred in the form of droplets of varying diameter between 250 nm and 250 µm. These droplets were confirmed to contain fluorine markers. Large droplets can be seen spread across the crystal in Fig. 10 (a), and smaller droplets are visible in Fig. 10 (b).

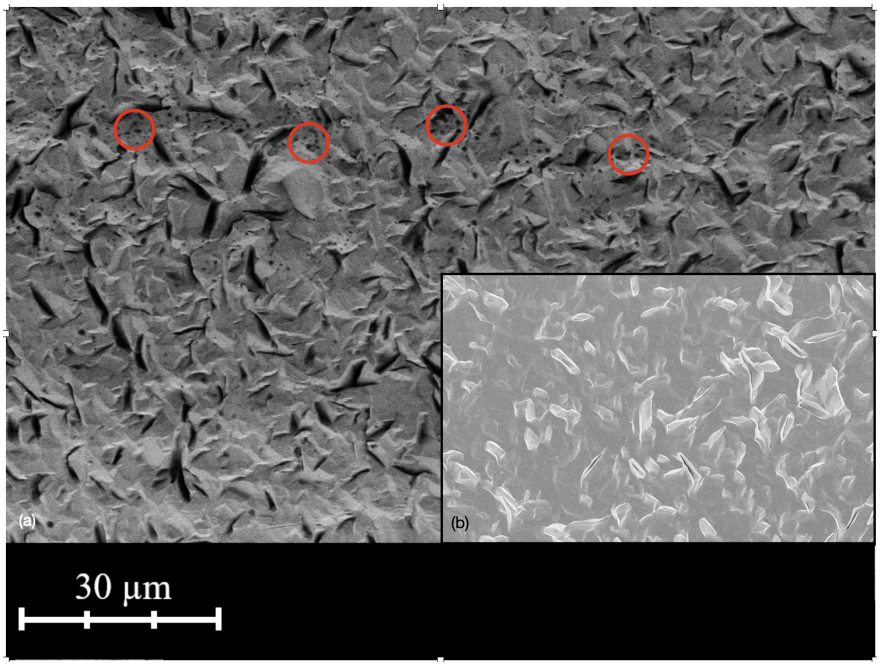

Fig. 9 (a) High energy (1,500x) with visual indications of deposition, (b) blank QCM crystal (1,500x) without any deposition.

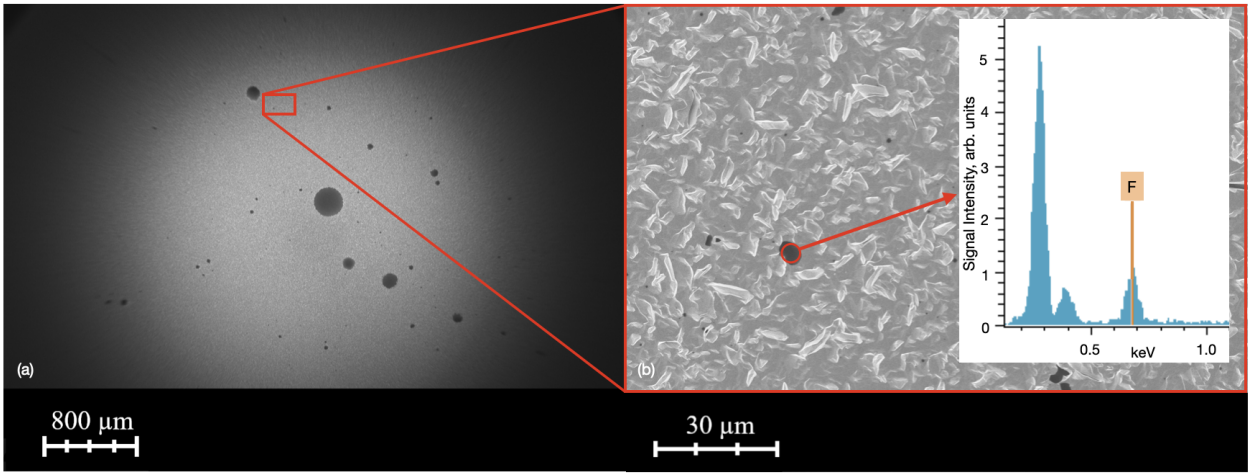

Fig. 10 (a) Low energy crystal (40x), (b) Low magnification (1,300x).

Droplets smaller than 1 µm did not produce meaningful EDX spectra. Though the droplet show in Figure 11 is thought to be EMI-BF_4, the fluorine marker is not detected above noise levels. This result could be due to the relative size of the droplet compared with the excitation area (1 µm) which would explain the prominent Au peak. Other effects such as electrons tunneling through the surface contaminate could explain the weak fluorine signal.

Figure 12 (a) shows two clear regions of the high energy sample, also seen in Fig. 4 (a). Figure 12 (b) and (c) show that both regions contain EMI-BF_4. The light appears to contain less deposited EMI-BF_4 than the dark region. It is not known exactly why the darker region contains more deposition than the exposed region, but this phenomenon will be explored in future work.

EDX is an easily accessible method for surface contamination detection, however, it is not without limitations. It is highly dependent on the area of the contamination and the thickness of that contamination. When surface features are smaller in area than the excitation area, X-rays from other parts of the sample can overwhelm marker signals as

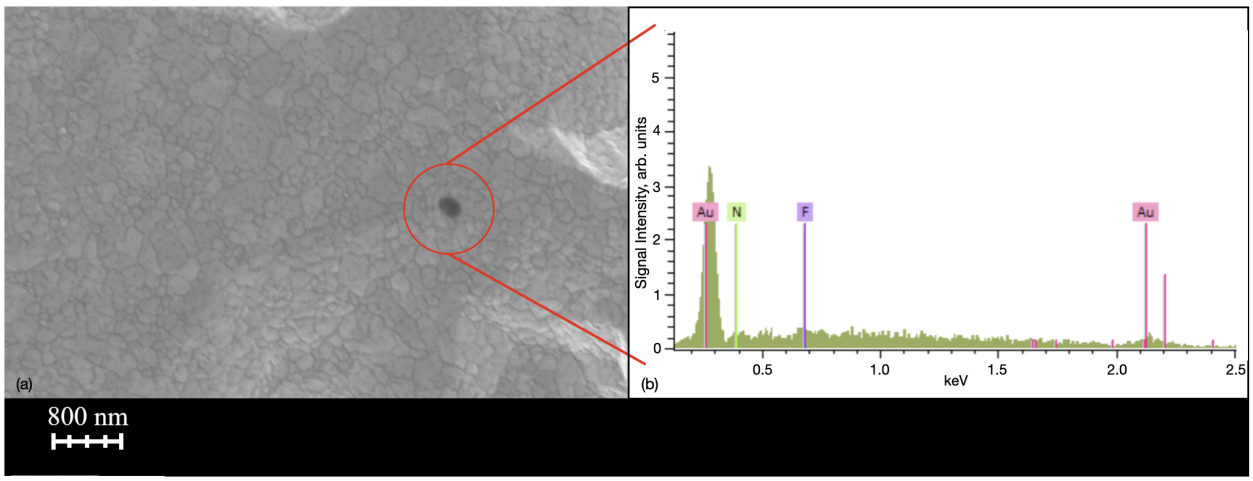

Fig. 11 (a) High magnification (30,000x) deposition of low energy EMI-BF_4, (b) EDX spectrum of the indicated region showing only minor counts of fluorine above background.

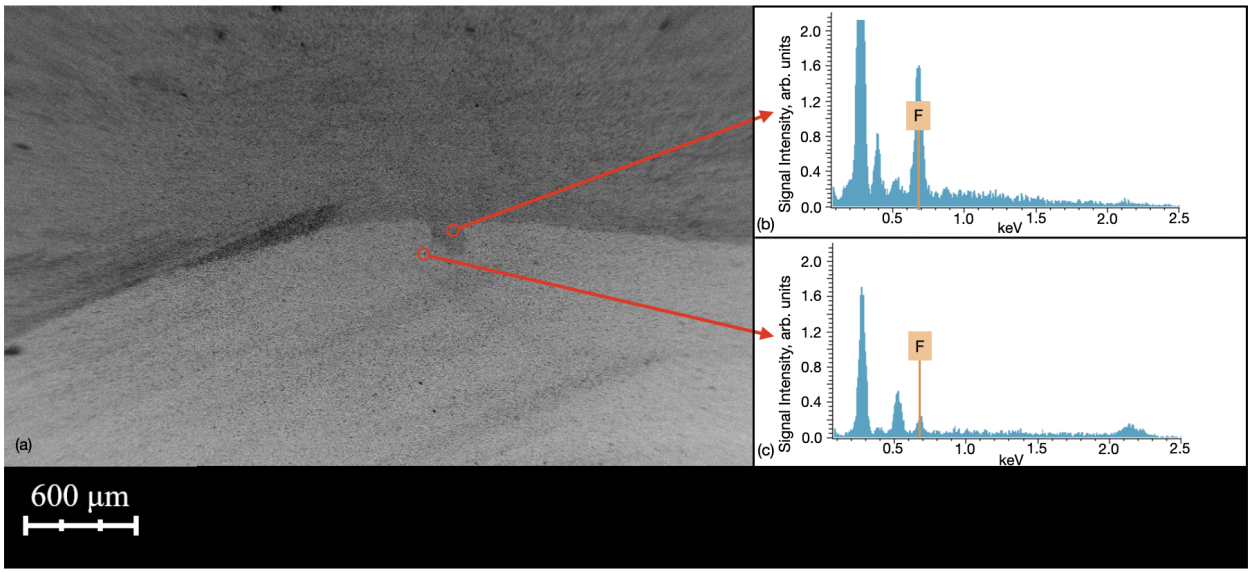

Fig. 12 (a) High energy sample (50x) with two regions visible, (b) EDX spectrum of the dark region showing a strong fluorine signal, (c) EDX spectrum of the light region showing a weaker fluorine signal.

seen in Fig. 11. While the ultimate feature size is dependent on the particular EDX machine in use, this technique will always produce less desirable results on features smaller than the excitation area. Additionally, in sparsely contaminated samples the subsurface penetration of electrons in EDX may be undesirable. Electrons may tunnel through the sparse contamination layer and excite X-rays from the substrate beneath giving the impression that the contamination is not present.

Despite these limitations in resolving the smallest areas of contamination, EDX proved effective in detecting fluorine in both high and low energy samples. The high energy sample produced smaller droplets than the low energy samples but as shown in Fig. 12 the smaller droplets still produced prominent fluorine peaks indicating the presence of EMI-BF_4.

C. NVR

1. Preliminary Study

Electrospray ionization (ESI) TOF-MS demonstrated the ability to detect EMI-BF_4 dissolved in a solution with a concentration of 64 µM, corresponding to 630 ng of EMI-BF_4 over a firing time of 5 minutes. This experiment indicates that using mass spectrometry on a rinse of a surface is likely a viable means of detection. Figure 13 shows the ability of the ESI TOF-MS to detect both the positive and negative ions from about 50 µL of the 64 µM EMI-BF_4 solution.

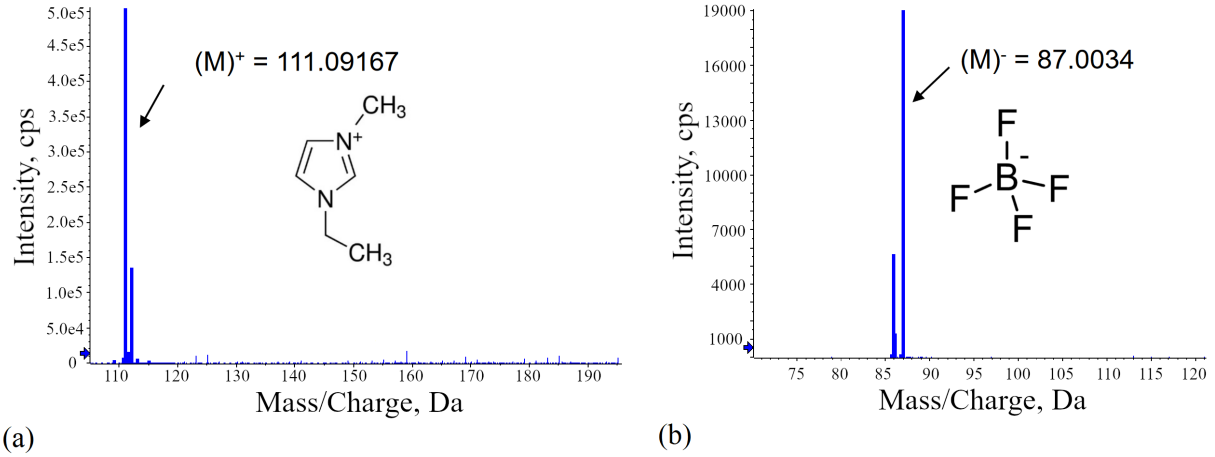

Fig. 13 (a) TOF-MS of EMI-BF_4 in the positive mode with a 64 µM concentration. (b) negative mode

2. Exposed Samples

The NVR samples were prepared by dissolving surface contaminates from the high and low energy samples with a rinse of approximately 5 mL of acetone, reducing down by allowing the solvent to evaporate, and reconstituting the residue into a known volume of solvent. This solution is loaded into an electrospray mass spectrometer to determine its molecular composition. Multiple Reaction Monitoring chromatography techniques (MRM) of a known concentration of EMI-BF_4 enables the estimation of the concentration of the solution rinses of the three samples. By estimating the concentration, the deposited mass can easily be obtained.

Table 1 shows the approximate mass of both the cations and anions rinsed from each sample. Though the cations make up most of the mass rinsed from each sample, roughly 25% more anions were present in the low energy sample rinse, and roughly 10% more anions were in the high energy rinse, this discrepancy is due to the lower molecular weight of the anion. Since the high and low energy crystals were exposed to a negative mode electrospray plume, finding a larger population of anions was expected.

Only a very small fraction of the total approximated emitted propellant mass from each test was found in these rinses. Molecular dynamics simulations predict that EMI-BF_4 ions do not tend to deposit for energies greater than 1 eV [11]. Furthermore, this difference could be the result of compounding factors including the interception of propellant on other surfaces during firing and poor rinsing efficiency. A significant amount of propellant, of both ions, was found on the unexposed crystal serving as a control. We hypothesize that this crystal was likely contaminated while under vacuum in the SEM with the exposed samples.

Table 1 Approximate mass of deposited propellant

Sample	Mass of positive ion (pg)	Mass of negative ion (pg)	Total propellant mass (pg)
Low energy	173	169	342
High energy	409	356	765
Control	65	95	160

D. FTIR

The liquid EMI-BF_4 sample was loaded into the FTIR, and an ATR-FTIR scan was performed on the bulk liquid. EMI-BF_4 was not available in the machine's database; however, 1-Butyl-3-methylimidazolium tetrafluoroborate (BMI-BF_4) closely matches. Figure 14 shows that these two molecules are very similar. This similarity is due to only a small number of chemical bond differences between the two. For ATR-FTIR measurements, a smooth or IR-transparent substrate must be used. Because of this requirement and time constraints, FTIR was not performed on any of the exposed samples.

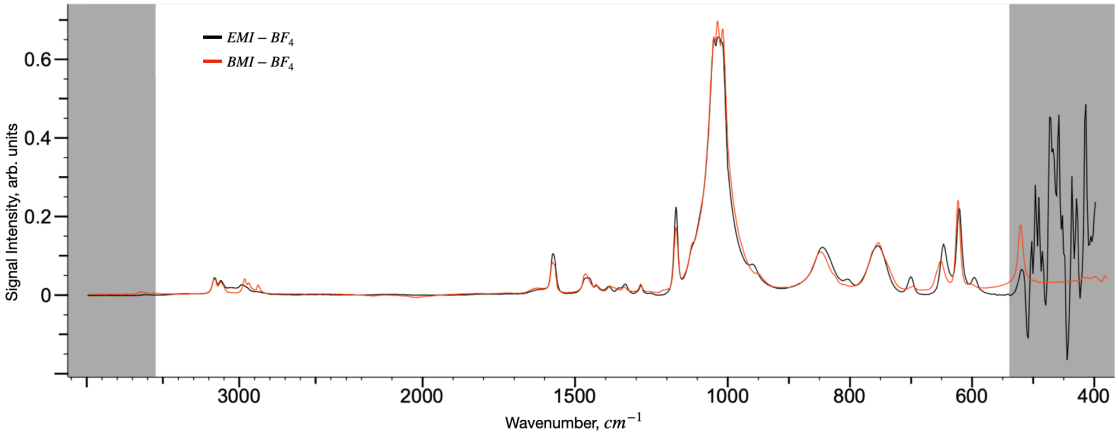

Fig. 14 ATR-IR Spectrum of EMI-BF_4, compared against BMI-BF_4

IV. Conclusion

This work describes four methods of detecting EMI-BF_4, fluorescence spectroscopy, EDX, NVR, and FTIR. Three of these methods were evaluated under three conditions of deposition- high energy, low energy, and no exposure. These conditions replicated expected environments that surfaces may be exposed to during the operation of an electrospray thruster, as well as different challenges for establishing detection. Future studies on fluorescent spectroscopy are required to fully understand the effect of EMI-BF_4 on a substrate's fluorescent signal.

Fluorescence spectrsocopy was not sensitive to the presence of EMI-BF_4, despite fluorescing strongly in the bulk fluid. This method, if proven capable of detection, exposes a region of about 2 mm^2 to the light, is quick, and does not require overly complicated instruments.

EDX is highly sensitive to EMI-BF_4, and is capable of detecting particles of EMI-BF_4 above 1 µm reliably via its fluorine signal. However, EDX cannot do broad area detection quickly, requires a ultra-high vacuum chamber, and is not capable of handling samples larger than a few inches.

NVR demonstrated a strong signal with 630 ng of EMI-BF_4 detected through ESI TOF-MS, indicating that the detection threshold is much more dilute than presently tested. Additionally, NVR is the only technique explored in this work to give an estimate of the mass deposited on each sample. This technique is highly sensitive, the data is collected over a short period of time, and uses a slightly modified capability that is accessible in a university environment. NVR must be performed as a last diagnostic because it is destructive to the deposition and gives no deposition structure information.

V. Future Work

Initial results are promising with regard to detection of EMI-BF_4 using a variety of means. Future work will be performed to quantify the limits of detection for each method, and add additional techniques. Fluorescence spectroscopy will be performed with other propellants and substrates to explore concrete explanations to the results found.

For NVR, further investigation into the efficiency of the solvent rinse is required to verify how accurate the measurements are to total deposition. This could be characterized using the SEM/EDX to observe the surface after performing a rinse.

Another technique of detection, Auger electron spectroscopy (AES), will be explored through future work. AES operates under similar properties to EDX, but is less prone to electron tunneling [12]. Initial results from Moog, Inc. demonstrate that AES is capable of measuring all non-hydrogen elements, including boron, in the bulk fluid, whereas EDX could only reliably measure fluorine. Future work will be performed to determine the limits of detection for AES using deposition from an electrospray source.

FTIR demonstrated the ability to produce a characteristic spectrum for EMI-BF_4, but further work is required to deposit EMI-BF_4 onto a substrate transparent to FTIR to confirm the ability of FTIR to detect trace amounts of EMI-BF_4.

The experiment will be extended to explore the feasibility of gas-phase fluorescence using the laser spectrophotometer, which has the promising ability to enable laser-induced fluorescent imaging and diagnostic insight to the ion plume.

VI. Acknowledgements

This work made use of the Cornell Center for Materials Research Shared Facilities which are supported through the NSF MRSEC program (DMR-1719875).

We thank Dr. S. Zhang of the Proteomics and Metabolomics Facility (RRID:SCR_021743) of the Biotechnology Resource Center of Cornell Institute of Biotechnology for their help with NVR mass spectrometer measurements.

This work was supported by the NASA Space Technology Graduate Research Opportunity.

We thank Monika Lukaczynska-Anderson and Jason Jones of Moog, Inc. for their generous Auger Electron Spectroscopy data.

References

[1] Thuppul, A., Wright, P. L., Collins, A. L., et al., "Lifetime Considerations for Electrospray Thrusters," *AIAA Propulsion and Energy 2019 Forum*, 19-22 August 2019. https://doi.org/10.2514/6.2019-3816.

[2] Krejci, D., Mier-Hicks, F., Thomas, R., et al., "Emission Characteristics of Passively Fed Electrospray Microthrusters with Propellant Reservoirs," *Journal of Spacecraft and Rockets*, Vol. 54, No. 2, March-April 2017. https://doi.org/10.2514/1.A33531.

[3] Petro, E. M., Gallud, X., Hampl, S. K., et al., "Multiscale modeling of electrospray ion emission," *J. Appl. Phys. 131, 193301*, 16 May 2022. https://doi.org/10.1063/5.0065615.

[4] Farnell, C. C., Farnell, C. C., Farnell, S. C., et al., "Electrostatic Analyzers with Application to Electric Propulsion Testing," *IEPC-2013-300*, October 6-10, 2013.

[5] Lakowicz, J., *Principles of Fluorescence Spectroscopy*, Springer US, 2007. URL https://books.google.com/books?id=-PSybuLNxcAC.

[6] Undavalli, V. K., Ling, C., and Khandelwal, B., "Chapter 6 - Impact of alternative fuels and properties on elastomer compatibility," *Aviation Fuels*, edited by B. Khandelwal, Academic Press, 2021, pp. 113–132. https://doi.org/https://doi.org/10.1016/B978-0-12-818314-4.00001-7.

[7] Tuladhar, R., and Yin, S., "4 - Production of recycled polypropylene (PP) fibers from industrial plastic waste through melt spinning process," *Use of Recycled Plastics in Eco-efficient Concrete*, edited by F. Pacheco-Torgal, J. Khatib, F. Colangelo, and R. Tuladhar, Woodhead Publishing Series in Civil and Structural Engineering, Woodhead Publishing, 2019, pp. 69–84. https://doi.org/https://doi.org/10.1016/B978-0-08-102676-2.00004-9.

[8] Collins, A. L., Wright, P. L., Uchizono, N. M., et al., "Neutral Mass Flux Measurements of an Electrospray Plume," *IEPC-2022-227*, June 19-23, 2022.

[9] Geiger, C. J., Bell, S., Chadwick, A., et al., "Energy-Dependent QCM Measurements of an Electrospray Plume," *IEPC-2022-227*, June 19-23, 2022.

[10] Lozano, P., and Martínez-Sánchez, M., "Ionic liquid ion sources: characterization of externally wetted emitters," *Journal of Colloid and Interface Science*, Vol. 282, No. 2, 2005. https://doi.org/https://doi.org/10.1016/j.jcis.2004.08.132.

[11] Bendimerad, R., and Petro, E., "Molecular dynamics studies of ionic liquid-surface interactions for electrospray thrusters," *Journal of Electric Propulsion*, Vol. 1, No. 27, 2022. https://doi.org/https://doi.org/10.1007/s44205-022-00032-9.

[12] Ilyin, A. M., "Chapter 11 - Auger Electron Spectroscopy," *Microscopy Methods in Nanomaterials Characterization*, edited by S. Thomas, R. Thomas, A. K. Zachariah, et al., Micro and Nano Technologies, Elsevier, 2017, pp. 363–381. https://doi.org/https://doi.org/10.1016/B978-0-323-46141-2.00011-0.